Beamforming Optimization for Intelligent Reflecting Surface-Aided MISO Communication Systems

Jung-Chieh Chen, *Member, IEEE*

***Abstract*—This article considers an intelligent reflecting surface (IRS)-assisted point-to-point multiple-input single-output communication system. An IRS implemented by configurable phase shifters is used to assist the transmission from an access point (AP) equipped with multiple antennas to a user having a single antenna. We aim to jointly optimize the transmit beamforming at the AP and the reflect beamforming at the IRS to maximize the spectral efficiency of the system. The considered joint optimization problem can be decoupled into the transmit and reflect beamforming design problems by applying the maximum-ratio transmission strategy. The former has a closed-form expression, whereas the latter requires solving a nonconvex optimization problem. A known solution based on manifold optimization (MO) is proposed to solve the reflect beamforming design problem. Although the MO-based algorithm achieves higher spectral efficiency than the conventional semidefinite relaxation approach, it incurs high time complexity. On this basis, we address this issue by proposing a computationally efficient gradient projection (GP)-based algorithm for the reflect beamforming design problem. When low-resolution (e.g., 1–2 bits) phase shifters are adopted, we leverage an innovative probability learning technique on the basis of the cross-entropy (CE) framework to alleviate the performance loss caused by the use of low-resolution phase shifters. Simulation results demonstrate that the proposed GP-based algorithm nearly obtains the same spectral efficiency as the state-of-the-art MO-based algorithm at a low complexity. However, the running time is significantly reduced. When low-resolution phase shifters are employed, the proposed CE-based algorithm outperforms the test algorithms in terms of spectral and energy efficiency in various system configurations.**

***Index Terms*—Beamforming optimization, cross-entropy, gradient projection, spectral efficiency, intelligent reflecting surface.**

I. Introduction

INTELLIGENT reflecting surfaces (IRSs), which are composed of a large number of low-cost passive reflecting elements, have received great interest in academia and industry on account of their potential to create favorable wireless environments by appropriately adjusting the weights of the reflecting elements [1]–[4]. In contrast to the conventional amplify-and-forward relaying technologies that require power amplifiers to retransmit the signal received from the access point (AP), IRSs passively reflect the incident signal from the AP and do *not* amplify or introduce noise. The power consumption levels of IRSs are much lower than the those of conventional amplify-and-forward relaying technologies because *no* amplifier is required. Moreover, the results of [2] showed that by carefully designing each reflecting element of an IRS, the IRS-aided scheme can remarkably improve the energy efficiency relative to conventional amplify-and-forward relaying technologies. Furthermore, IRSs can be easily deployed and merged into existing wireless communication systems. Because of these distinguishable features, the IRSs have been explored in various communication applications, for example, physical layer security [5]–[8], wireless power transfer [9]–[12], and multigroup multicast [13].

A. Relevant Prior Art

Recently, several studies have been proposed to improve the spectral efficiency of the IRS-assisted single-user multiple-input single-output (MISO) downlink system by simultaneously designing the transmit beamforming at the AP and the reflect beamforming at the IRS [14]–[17]. However, the reflecting elements of the IRSs are realized by phase shifters, in which only the phases of the incident signals can be adjusted. Accordingly, the constant magnitude imposed on the phase shifters makes the optimal reflect beamforming design problem intractable. The joint design of the transmit and reflect beamforming is challenging due to the use of a large number of reflecting elements at the IRS. To tackle this joint optimization problem, the studies in [14], [15] proposed the application of the maximum-ratio transmission strategy to decouple the joint optimization problem into the transmit and reflect beamforming design problems. The former has a closed-form expression, while the latter requires solving a nonconvex optimization problem. The studies in [14], [15] further applied the semidefinite relaxation (SDR) approach to solve the reflect beamforming design problem. However, the SDR approach incurs high complexity. This approach only provides an approximate solution. On this basis, the work in [16] exploited the manifold optimization (MO) technique to address the reflect beamforming design problem. The results of [16] show that the MO-based algorithm not only significantly performs better than the SRD-based algorithm but also requires much less running time than the SRD-based algorithm. To achieve a high performance, reference [17] applied a branch-and-bound (BnB) algorithm to solve the reflect beamforming design problem. Although the BnB-based algorithm can obtain a globally optimal

Manuscript received August 15, 2020; revised November 2, 2020; accepted November 26, 2020. Date of publication December 22, 2020; date of current version February 12, 2021. This work was supported in part by the Ministry of Science and Technology (MOST) of Taiwan under Grant MOST 109-2221-E-017-009. The review of this article was coordinated by Dr. H. Lin.

The author is with the Department of Electrical Engineering, National Kaohsiung Normal University, Kaohsiung 80 201, Taiwan (e-mail: jcchen@nknucc.nknu.edu.tw).

Digital Object Identifier 10.1109/TVT.2020.3046271

solution, its high computational complexity restricts its use for large-scale IRS systems.

B. Motivation and Contributions

On the basis of the results of [17], the MO-based algorithm can offer comparable spectral efficiency to the BnB-based algorithm at a low computational cost. Therefore, the MO-based algorithm is applicable for designing large-scale IRS systems, because it can yield a favorable trade-off between complexity and spectral efficiency. To the best of our knowledge, the MO-based algorithm achieves the *highest* spectral efficiency of all existing approaches for *large-scale* IRS systems. However, the MO-based algorithm presents two challenges: (1) the required time and computational complexities of the MO-based algorithm remain high; (2) the aforementioned studies [14]–[17] have assumed that infinite-resolution phase shifters are used to generate any required phase. However, in practice, phase shifters have finite resolution. Therefore, this study concentrates on the IRS-assisted single-user MISO downlink system to address these issues. The key results and contributions of this study are summarized as follows.

1) *A computationally efficient algorithm for designing reflect beamforming with infinite-resolution phase shifters:* We propose a computationally efficient gradient projection (GP)-based algorithm to tackle the reflect beamforming design problem to reduce the time and computational complexities of the MO-based algorithm while maintaining the spectral efficiency. Given that the proposed GP-based algorithm comprises only the gradient and projection steps, its complexity is significantly lower than that of the MO-based algorithm. We show that the value of the objective function monotonically decrease by properly selecting a stepsize of the proposed GP-based algorithm, thereby ensuring that the proposed GP-based algorithm will converge to a desired solution.
2) *An effective algorithm to mitigate the performance loss caused by the use of low-resolution phase shifters for the reflect beamforming design problem:* In practice, the reflecting elements of the IRSs are implemented with *finite*-resolution phase shifters. Although we can directly quantize each continuous phase shifter obtained by the MO-based or the GP-based algorithm to a feasible set, such a direct quantization approach causes significant performance loss when 1-bit phase shifters are employed. To alleviate performance loss due to the use of low-resolution phase shifters, the authors in [18], [19] have applied an alternating optimization (AO)-based technique to design their reflect beamforming. Even though the AO-based algorithm can mitigate the performance loss caused by coarse 1-bit phase shifters, its performance can still be improved. Moreover, for 2-bit phase shifters, the performance of the AO-based algorithm is inferior to that of the direct quantization approaches. In this study, we leverage an innovative probability learning technique based on the cross-entropy (CE) framework [20] to reduce the performance loss caused by the use of 1-bit phase shifters. Here, an explicit expression is derived for updating the learning parameters of the proposed CE-based algorithm, thus facilitating fast evaluation.
3) *Superior performance:* Simulation results reveal that the proposed GP-based algorithm not only possesses low complexity but also delivers nearly the same spectral efficiency as the state-of-the-art MO-based algorithm when the reflecting elements of the IRSs are implemented using infinite-resolution phase shifters. The required running time of the proposed GP-based algorithm can be significantly reduced. When low-resolution phase shifters are employed, the proposed CE-based algorithm can achieve higher spectral and energy efficiency than those of the test algorithms for various system configurations. Most importantly, simulation results reveal that the proposed GP-based and CE-based algorithms can still be applied for imperfect channel state information (CSI) because their performance degradation is small.

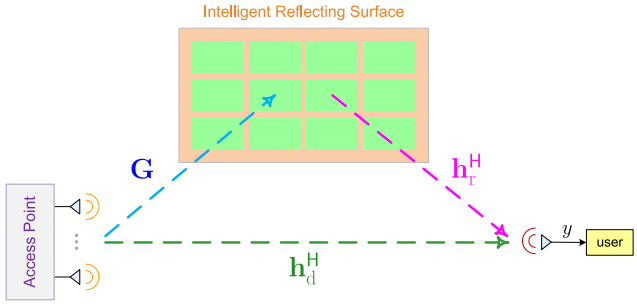

Fig. 1. IRS-assisted downlink system, where the AP has M antennas, the user is equipped with a single antenna, and the IRS is implemented by N configurable phase shifters.

Notations: $\mathbb{R}$ and $\mathbb{C}$ represent the set of real numbers and complex numbers, respectively; superscripts $(\cdot)^\top$ and $(\cdot)^\mathsf{H}$ denote the transpose and Hermitian transpose, respectively; $\mathrm{E}\{\cdot\}$ represents the expectation operator; $\lceil\cdot\rceil$ is the ceiling operation; $\measuredangle$ denotes the associated phase; $|\cdot|$ denotes the cardinality of a given set; $\mathrm{diag}(\mathbf{x})$ represents the diagonal matrix with the vector $\mathbf{x}$ on its diagonal; $\mathcal{N}_\mathbb{C}(0,\sigma^2)$ represents a complex Gaussian distribution with zero-mean and variance σ^2; $\sim$ means "is distributed according to;" and j denotes the imaginary unit, i.e., $\mathrm{j}=\sqrt{-1}$.

II. System Model and Problem Formulation

Following the system model of recent state-of-the-art works on IRS-aided communication systems [14]–[17], we consider an IRS-assisted MISO downlink communication system. As shown in Fig. 1, an IRS implemented by N configurable phase shifters is used to assist the transmission from an M-antenna AP to a single-antenna user. At the AP, the information-bearing symbol s with $\mathrm{E}\{|s|^2\}=1$ is precoded by a linear beamforming vector $\mathbf{f}\in\mathbb{C}^{M\times 1}$ to create a transmit vector $\mathbf{f}s\in\mathbb{C}^{M\times 1}$. Then, the received signal at the user can be written as

$$y=\left(\mathbf{h}_\mathrm{r}^\mathsf{H}\boldsymbol{\Phi}\mathbf{G}+\mathbf{h}_\mathrm{d}^\mathsf{H}\right)\mathbf{f}s+z, \tag{1}$$

where $\mathbf{h}_{\mathrm{d}}^{\mathsf{H}} \in \mathbb{C}^{1\times M}$, $\mathbf{h}_{\mathrm{r}}^{\mathsf{H}} \in \mathbb{C}^{1\times N}$, and $\mathbf{G} \in \mathbb{C}^{N\times M}$ denote the baseband equivalent channels from the AP to the user, from the IRS to the user, and from the AP to the IRS, respectively; and z is the additive complex Gaussian noise with zero mean and variance σ^2. Moreover, $\mathbf{\Phi} \triangleq \mathrm{diag}(\mathbf{x})$ with $\mathbf{x} = [e^{\mathrm{j}\theta_1}, \ldots, e^{\mathrm{j}\theta_N}]^\top$ is the passive reflect beamforming matrix at the IRS, where θ_n is the phase shift of the n-th reflection element of the IRS. Based on (1), the spectral efficiency is given by

$$\mathsf{R}(\mathbf{f}, \mathbf{\Phi}) = \log\left(1 + \frac{\left|\left(\mathbf{h}_{\mathrm{r}}^{\mathsf{H}}\mathbf{\Phi}\mathbf{G} + \mathbf{h}_{\mathrm{d}}^{\mathsf{H}}\right)\mathbf{f}\right|^2}{\sigma^2}\right). \tag{2}$$

This study aims to jointly design the transmit beamforming vector $\mathbf{f}$ and the reflect beamforming matrix $\mathbf{\Phi}$ that maximizes (2). Mathematically, the considered joint design problem can be formulated as [15]

$$(\mathbf{P1}):\ \underset{\mathbf{f},\mathbf{\Phi}}{\text{maximize}} \quad \left|\left(\mathbf{h}_{\mathrm{r}}^{\mathsf{H}}\mathbf{\Phi}\mathbf{G} + \mathbf{h}_{\mathrm{d}}^{\mathsf{H}}\right)\mathbf{f}\right|^2 \tag{3a}$$

$$\text{subject to} \quad \|\mathbf{f}\|^2 \le P, \tag{3b}$$

$$\theta_n \in [0, 2\pi), \ \text{for } n = 1, \ldots, N, \tag{3c}$$

where P is the given total transmit power. Problem (3) is intractable because of the coupling of $\mathbf{f}$ and $\mathbf{\Phi}$. Nevertheless, problem (3) can be decoupled into the transmit and reflect beamforming design problems by applying the maximum-ratio transmission strategy. The optimal transmit beamforming solution is given by [15]

$$\mathbf{f} = \sqrt{P}\frac{\mathbf{G}^{\mathsf{H}}\mathrm{diag}(\mathbf{h}_{\mathrm{r}})\mathbf{x} + \mathbf{h}_{\mathrm{d}}}{\|\mathbf{G}^{\mathsf{H}}\mathrm{diag}(\mathbf{h}_{\mathrm{r}})\mathbf{x} + \mathbf{h}_{\mathrm{d}}\|_2}. \tag{4}$$

However, the optimal reflect beamforming vector $\mathbf{x}$ still needs to be determined. On the basis of [16], determining the optimal $\mathbf{x}$ requires solving the following optimization problem:

$$(\mathbf{P2}):\ \underset{\mathbf{x}}{\text{minimize}} \quad f(\mathbf{x}) = -\mathbf{x}^{\mathsf{H}}\mathbf{A}\mathbf{x} - \mathbf{x}^{\mathsf{H}}\mathbf{b} - \mathbf{b}^{\mathsf{H}}\mathbf{x} \tag{5a}$$

$$\text{subject to} \quad \mathbf{x} \in \mathcal{S}, \tag{5b}$$

where $\mathcal{S} \triangleq \{\mathbf{x} \in \mathbb{C}^{N\times 1} : |x_1| = |x_2| = \cdots = |x_N| = 1\}$ is the unit-modulus constraint set, $\mathbf{A} \triangleq \mathrm{diag}(\mathbf{h}_{\mathrm{r}}^{\mathsf{H}})\mathbf{G}\mathbf{G}^{\mathsf{H}}\mathrm{diag}(\mathbf{h}_{\mathrm{r}})$, and $\mathbf{b} \triangleq \mathrm{diag}(\mathbf{h}_{\mathrm{r}}^{\mathsf{H}})\mathbf{G}\mathbf{h}_{\mathrm{d}}$. In practice, the phase shifter only has a finite resolution. If phase shifters with the α-bit resolution are used, then x_n is restricted to the values of $\mathcal{F}_\alpha \triangleq \{e^{\mathrm{j}\Delta}, e^{\mathrm{j}2\Delta}, \ldots, e^{\mathrm{j}2^\alpha\Delta}\}$, where $\Delta = \frac{2\pi}{2^\alpha}$ is the resolution of phase shifters. In this case, problem (5) can be recast as

$$(\mathbf{P3}):\ \underset{\mathbf{x}}{\text{minimize}} \quad f(\mathbf{x}) = -\mathbf{x}^{\mathsf{H}}\mathbf{A}\mathbf{x} - \mathbf{x}^{\mathsf{H}}\mathbf{b} - \mathbf{b}^{\mathsf{H}}\mathbf{x} \tag{6a}$$

$$\text{subject to} \quad x_n \in \mathcal{F}_\alpha, \ \text{for } n = 1, \ldots, N. \tag{6b}$$

Remark 1: Problem (5) is a nonconvex optimization problem owing to the unit-modulus constraints in (5b). Reference [16] addressed this problem by using the MO-based algorithm. The results showed that the MO-based algorithm provides excellent spectral efficiency that remarkably outperforms the SDR-based algorithm. However, the required computational and time complexities of the MO-based algorithm remain high. Therefore, we propose a GP-based algorithm to reduce the time and computational complexities of the MO-based algorithm without sacrificing the spectral efficiency in Section III.

Remark 2: Problem (6) can be solved by performing a brute-force search owing to the discrete nature of (6b). However, such a brute-force search is impracticable because its complexity exponentially grows with N (N is typically large). Although we can directly quantize each continuous phase shifter obtained by the MO-based algorithm to its nearest discrete value in $\mathcal{F}_\alpha$, such a direct quantization approach causes significant performance loss when 1-bit phase shifters are employed. Therefore, we propose a CE-based algorithm to lessen the performance loss caused by using 1-bit phase shifters in Section IV.

III. GP-Based Algorithm for Designing Reflect Beamforming With Infinite-Resolution Phase Shifters

The gradient descent scheme is a computationally efficient approach for solving the optimization problems. However, this scheme *cannot* guarantee that the obtained solution is feasible for constrained optimization problems. To address this issue, the GP framework projects the solution obtained by the gradient descent method into the constraint set. Specifically, the update rule of the GP framework for each iteration t for problem (5) is given by [21]

$$\mathbf{x}^{(t+1)} = \Pi_{\mathcal{S}}[\mathbf{x}^{(t)} - \mu\nabla f(\mathbf{x}^{(t)})], \tag{7}$$

where μ is a pre-specified stepsize and $\nabla f(\mathbf{x}^{(t)}) = -2(\mathbf{A}\mathbf{x}^{(t)} + \mathbf{b})$ is the gradient of the objective function in (5a). In addition, $\Pi_{\mathcal{S}}(\cdot)$ is the projection operator that projects the input onto the unit-modulus constraint set $\mathcal{S}$. This projection operator can be considered a phase-extraction operation and admits a closed-form solution given by $\Pi_{\mathcal{S}}(\mathbf{x}^{(t)}) = e^{\mathrm{j}\angle\mathbf{x}^{(t)}}$. Hence, the GP framework for solving problem (5) consists of the following two update procedures, which are executed for each iteration t:

$$\boldsymbol{\zeta}^{(t+1)} = \mathbf{x}^{(t)} + 2\mu\left(\mathbf{A}\mathbf{x}^{(t)} + \mathbf{b}\right), \tag{8a}$$

$$\mathbf{x}^{(t+1)} = e^{\mathrm{j}\angle\boldsymbol{\zeta}^{(t+1)}}, \tag{8b}$$

where the algorithm is discontinued if $|f(\mathbf{x}^{(t)}) - f(\mathbf{x}^{(t+1)})| \le \varepsilon$. This procedure is illustrated in Algorithm 1.

Although directly projecting the solution obtained by the gradient descent method into a unit modulus constraint in (8b) can guarantee that the resulting solution is feasible, such a projection operator may cause a convergence problem. However, this issue can be addressed by carefully choosing the stepsize, as stated in the following proposition.

Proposition 1: Let $\lambda_{\max}$ be the maximum eigenvalue of $\mathbf{A}$. If $\{\mathbf{x}^{(t)}\}$ is the sequence of feasible solutions generated by the GP algorithm, and $\mu \le \frac{1}{4\lambda_{\max}}$, then $f(\mathbf{x}^{(t+1)}) \le f(\mathbf{x}^{(t)})$.

Proof: See Appendix A. ■

Remark 3: The complexity of Algorithm 1 is dominated by the computation of $\widetilde{\mathbf{A}}\mathbf{x}^{(t)}$, which involves matrix-vector multiplications with a complexity order of $\mathcal{O}(N^2)$. Accordingly, the total complexity of Algorithm 1 is $\mathcal{O}(N^2 t_{\max})$, where $t_{\max}$ is the number of iterations required to meet a stopping criterion. By contrast, the MO-based algorithm is a four-step iterative

Algorithm 1: GP-based algorithm for problem (5)

Input: $\mathbf{A}$ and $\mathbf{b}$

1 Initialization: Set $t=0$, $\mu=\frac{1}{4\lambda_{\max}}$, $\mathbf{x}^{(0)}\in\mathcal{F}_\kappa^N$, $\widetilde{\mathbf{A}}=2\mu\mathbf{A}$, $\widetilde{\mathbf{b}}=2\mu\mathbf{b}$;

2 **repeat**

3 $\quad\boldsymbol{\zeta}^{(t+1)}\leftarrow\mathbf{x}^{(t)}+\widetilde{\mathbf{A}}\mathbf{x}^{(t)}+\widetilde{\mathbf{b}}$;

4 $\quad\mathbf{x}^{(t+1)}\leftarrow e^{\mathrm{j}\measuredangle\boldsymbol{\zeta}^{(t+1)}}$;

5 $\quad t\leftarrow t+1$;

6 **until** $|f(\mathbf{x}^{(t)})-f(\mathbf{x}^{(t+1)})|\le\varepsilon$;

Output: $\mathbf{x}^{(t)}$

algorithm, which involves gradient, projection, retraction, vector transport, and conjugate direction on the manifold for each iteration. On the basis of the similar analysis in [22], the total complexity of the MO-based algorithm is approximately $\mathcal{O}((3N^2+10N)t_{\max})$.

IV. CE-Based Algorithm for Designing Reflect Beamforming With Finite-Resolution Phase Shifters

In this section, we investigate how to apply the CE framework for problem (6). The CE framework is a two-step iterative probability learning technique that begins with a sampling distribution parameterized by tilting parameters. In the first step of each iteration, a set of random solutions is generated from this sampling distribution, where the fixed number of high-ranking solutions represents the *elite* samples. In the second step of each iteration, the elite samples are used to update the tilting parameters of the sampling distribution to generate better solutions in the next iteration. The optimal updating rule for the tilting parameters is found by solving a cross-entropy minimization problem [20]. Refer to [20] for a comprehensive review of the CE methods.

We let $X_1,\ldots,X_N$ be the independent discrete random variables to generate feasible solutions for problem (6), where the outcome of X_n, denoted by x_n, can only take the values $e^{\mathrm{j}\Delta}$, $e^{\mathrm{j}2\Delta}$, …, $e^{\mathrm{j}2^\alpha\Delta}$. The probability distribution of X_n is $\Pr\{X_n=e^{\mathrm{j}k\Delta}\}=p_{nk}$ for $k=1,\ldots,|\mathcal{F}_\alpha|$, where p_{nk} denotes the probability of the k-th element in set $\mathcal{F}_\alpha$ being selected as x_n. We use a probability matrix $\mathbf{P}\triangleq[p_{nk}]\in\mathbb{R}^{N\times|\mathcal{F}_\alpha|}$ to determine which element in set $\mathcal{F}_\alpha$ should be assigned to which phase shifter. Sampling the elements out of $\mathcal{F}_\alpha$ independently for each phase shifter according to $\mathbf{P}$ leads to the probability of drawing a specific sample $\mathbf{x}$ as

$$\mathscr{P}(\mathbf{x};\mathbf{P})\triangleq\prod_{n=1}^{N}\sum_{k=1}^{|\mathcal{F}_\alpha|}p_{nk}\mathbb{1}_{\{\mathcal{I}_n(\mathbf{x})=e^{\mathrm{j}k\Delta}\}},\tag{9}$$

where $\mathbb{1}_{\{\cdot\}}$ is an indicator function, and $\mathcal{I}_n(\mathbf{x})\triangleq x_n$ is a function used to identify the n-th element from the vector $\mathbf{x}$.

The CE iteration begins with an initial probability matrix $\mathbf{P}^{(0)}$. In the first step of each iteration t, we sample L candidate solutions $\{\mathbf{x}_\ell^{(t)}\}_{\ell=1}^L$ according to $\mathscr{P}(\cdot;\mathbf{P}^{(t-1)})$ given in (9) and then evaluate them on the basis of (6a) to obtain an objective value set $\{f(\mathbf{x}_\ell^{(t)})\}_{\ell=1}^L$. The generated solutions are sorted by their objective values in the ascending order as $f(\mathbf{x}_{[1]}^{(t)})\le\cdots\le f(\mathbf{x}_{[L]}^{(t)})$ to determine the best $L^{\text{elite}}\triangleq\lceil\varsigma L\rceil$ solutions with smallest objective values (i.e., elite samples), where $f(\mathbf{x}_{[\ell]}^{(t)})$ is the ℓ-th smallest value of set $\{f(\mathbf{x}_{[\ell]}^{(t)})\}_{\ell=1}^L$ and $0<\varsigma<1$ is called the elite ratio. In the second step of each iteration t, we update the parameter matrix $\mathbf{P}$ only on the basis of the elite samples $\{\mathbf{x}_{[\ell]}^{(t)}\}_{\ell=1}^{L^{\text{elite}}}$. Proposition 2 provides the optimal update formula in the sense of the smallest Kullback–Leibler divergence.

Proposition 2: The optimal probability matrix $\mathbf{P}^{(t)}=[p_{nk}^{(t)}]$ that minimizes the Kullback–Leibler distance between the parameterized distribution and the target distribution composed of the elite solutions $\{\mathbf{x}_{[\ell]}^{(t)}\}_{\ell=1}^{L^{\text{elite}}}$ is

$$p_{nk}^{(t)}=\frac{1}{L^{\text{elite}}}\sum_{\ell=1}^{L^{\text{elite}}}\mathbb{1}_{\{\mathcal{I}_n(\mathbf{x}_{[\ell]}^{(t)})=e^{\mathrm{j}k\Delta}\}},\tag{10}$$

for $n=1,\ldots,N$ and $k=1,\ldots,|\mathcal{F}_\alpha|$.

Proof: See Appendix B. ■

Remark 4: We have a simple interpretation for (10). To update p_{nk}, we simply take the fraction of times that the k-th element in set $\mathcal{F}_\alpha$ is selected as x_n, taking into account only elite solutions.

Similar to other reinforcement learning methods, the CE-based algorithms apply a *smoothing* strategy to avoid premature convergence to local optima. Specifically, a fixed learning parameter $\beta\in(0,1]$ is applied to tilting parameters to slow down the convergence via

$$p_{nk}^{(t)}:=\beta\times p_{nk}^{(t)}+(1-\beta)\times p_{nk}^{(t-1)},\tag{11}$$

where $p_{nk}^{(t)}$ is the present update obtained by (10), while $p_{nk}^{(t-1)}$ is the smoothing update in the last iteration. Notably, by carefully selecting an appropriate learning parameter, the CE-based algorithms converge to the optimal solution with probability arbitrarily close to one [23]. In summary, we describe the detailed procedure of the proposed CE-based algorithm for solving problem (6) in Algorithm 2.

Remark 5: In each iteration, the complexity of Algorithm 2 mostly originates from the objective function calculation in Line 9, which requires the complexity order of $\mathcal{O}(2N(N+1))$ in each sample. The computational complexity of evaluating L candidate solutions is $\mathcal{O}(2N(N+1)L)$. In $t_{\max}$ iterations, the total computational complexity of Algorithm 2 is $\mathcal{O}(2N(N+1)Lt_{\max})$. In practice, $L=\varpi N$ is always suggested to be applied to achieve the desired performance [20], where ϖ is a constant that is greater than or equal to two. Accordingly, the parameter settings for Algorithm 2 in the simulation are set as $\varpi=2$, $\vartheta=0.65$, $\beta=0.1$, and $t_{\max}=30$ on the basis of the recommendation of [20]. The complexity of a brute-force search is $\mathcal{O}(2N(N+1)|\mathcal{F}_\alpha|^N)$, which is far higher than that of Algorithm 2.

Algorithm 2: CE-based for solving problem (6)

Input: Sample size L, parameter ς, and smoothing parameter β

$t \leftarrow 0$
$\mathbf{P}^{(t)} = [p_{nk}^{(t)}] \leftarrow [\frac{1}{|\mathcal{F}_\alpha|}]$
$L^{\text{elite}} \leftarrow \lceil \varsigma L \rceil$
$\mathtt{f}_{\text{best}} \leftarrow \infty$
$\mathbf{x}_{\text{best}} \leftarrow \varnothing$
while $t \leq t_{\max}$ **do**
  for $\ell = 1$ **to** L **do**
    Generate a random vector $\mathbf{x}_\ell^{(t)}$ from $\mathscr{P}(\cdot; \mathbf{P}^{(t-1)})$
    Calculate the objective $f(\mathbf{x}_\ell^{(t)})$ of $\mathbf{x}_\ell^{(t)}$ according to (6a)
  Ascending sorting $\{f(\mathbf{x}_\ell^{(t)})\}_{\ell=1}^{L}$ to $f(\mathbf{x}_{[1]}^{(t)}) \leq \cdots \leq f(\mathbf{x}_{[L^{\text{elite}}]}^{(t)}) \leq \cdots \leq f(\mathbf{x}_{[L]}^{(t)})$
  if $f(\mathbf{x}_{[1]}^{(t)}) < \mathtt{f}_{\text{best}}$ **then**
    $\mathtt{f}_{\text{best}} \leftarrow f(\mathbf{x}_{[1]}^{(t)})$
    $\mathbf{x}_{\text{best}} \leftarrow \mathbf{x}_{[1]}^{(t)}$
  for $n = 1$ **to** N **do**
    for $k = 1$ **to** $|\mathcal{F}_\alpha|$ **do**
      $p_{nk}^{(t)} \leftarrow \frac{1}{L^{\text{elite}}} \sum_{\ell=1}^{L^{\text{elite}}} \mathbb{1}_{\{\mathcal{I}_n(\mathbf{x}_{[\ell]}^{(t)}) = e^{\mathrm{j}k\Delta}\}}$
      $p_{nk}^{(t)} \leftarrow \beta \times p_{nk}^{(t)} + (1-\beta) \times p_{nk}^{(t-1)}$
  $t \leftarrow t + 1$

Output: $\mathbf{x}_{\text{best}}$

V. Simulation Results and Discussion

A. Simulation Settings

Our simulation environments are similar to those developed in [24], where the AP located at (0,0) has $M = 4$ antennas, the location of IRS is $(200\text{ m}, 0)$, and a single-antenna user is randomly located within a circle centered at $(200\text{ m}, 30\text{ m})$ with a radius of 10 m. The noise power at the user is set to $\sigma^2 = -170$ dBm/Hz. On the basis of the modeling guideline in the 3GPP propagation environment, the path-loss model for the line-of-sight (LoS) case and the non-LoS (NLoS) case are illustrated by [24]

$$\text{PL}(\delta)\,[\text{dB}] = \begin{cases} 35.6 + 22.0\log_{10}(\delta), & \text{for LoS}, \\ 32.6 + 36.7\log_{10}(\delta), & \text{for NLoS}, \end{cases} \tag{12}$$

where δ is the distance in meter. In this study, we assume that the LoS component is involved in the AP-IRS and the IRS-user channels. We also assume that $\mathbf{h}_{\text{d}}$ follows Rayleigh fading, while $\mathbf{G}$ and $\mathbf{h}_{\text{r}}$ follow Rician fading. The resulting $\mathbf{G}$ and $\mathbf{h}_{\text{r}}$ are modeled as

$$\mathbf{G} = \mathcal{L}_1 \left(\sqrt{\frac{\gamma}{\gamma+1}} \mathbf{a}_N(\vartheta)\mathbf{a}_M(\psi)^{\mathsf{H}} + \sqrt{\frac{1}{\gamma+1}} \bar{\mathbf{G}} \right), \tag{13}$$

$$\mathbf{h}_{\text{r}} = \mathcal{L}_2 \left(\sqrt{\frac{\gamma}{\gamma+1}} \mathbf{a}_N(\phi) + \sqrt{\frac{1}{\gamma+1}} \bar{\mathbf{h}}_{\text{r}} \right), \tag{14}$$

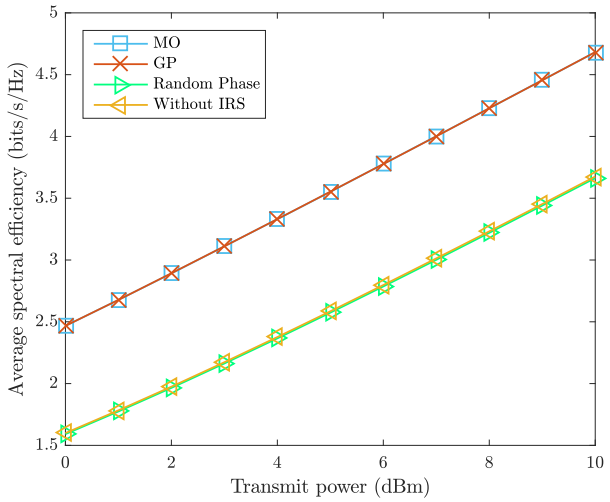

Fig. 2. Spectral efficiency versus transmit power for an IRS-assisted downlink system when $M = 4$ and $N = 100$.

where $\mathcal{L}_1$ and $\mathcal{L}_2$ are the corresponding path-losses; $\gamma = 10$ is the Rician factor; $\bar{\mathbf{G}}$ and $\bar{\mathbf{h}}_{\text{r}}$ are the NLoS components whose entries are modeled as $\mathcal{N}_{\mathbb{C}}(0,1)$; and $\mathbf{a}_M(\psi)$, $\mathbf{a}_N(\vartheta)$, and $\mathbf{a}_N(\phi)$ are the antenna array response vectors of a half-wavelength uniform linear array with ψ, ϑ, and ϕ being the angular parameters, respectively.

B. Continuous Reflecting Coefficients

We first investigate the spectral efficiency of the test algorithms by using infinite-resolution phase shifters. Fig. 2 shows the spectral efficiency as a function of transmit power for $N = 100$. In addition to the state-of-the-art MO-based algorithm [16],[1] we include two baselines for comparison: the random phase scheme and without the aid of IRS. The former optimizes the transmit beamforming $\mathbf{f}$ by using (4) with random phase shifts. The latter does not consider the IRS and directly applies the optimal transmit beamforming to align the beam to the direct channel $\mathbf{h}_{\text{d}}$ (i.e., $\mathbf{f} = \sqrt{P}\mathbf{h}_{\text{d}}/\|\mathbf{h}_{\text{d}}\|_2$). No performance gain is obtained for deploying the IRS if its phase vector is not optimized. However, the IRS-assisted wireless system can provide approximately 5 dB gain compared with the system without IRS by carefully optimizing the phase vector of IRS by using the MO-based algorithm. This result demonstrates the effectiveness of integrating IRSs into wireless communication systems. The proposed GP-based algorithm provides indistinguishable spectral efficiency performance from that of the MO-based algorithm in all transmit power region.

Next, we evaluate the performance of the MO-based and GP-based algorithms in terms of computational complexity and running time. Figs. 3 and 4 plot the convergence curve of the objective value (i.e., $f(\mathbf{x})$) versus the number of iterations and the running time, respectively, for the MO-based and GP-based algorithms when $P = 5$ dBm and $N = 100$. Here, the running

[1]The MO-based algorithm is chosen for comparison because, to the best of our knowledge, it achieves the highest spectral efficiency among all existing approaches for large-scale IRS systems.

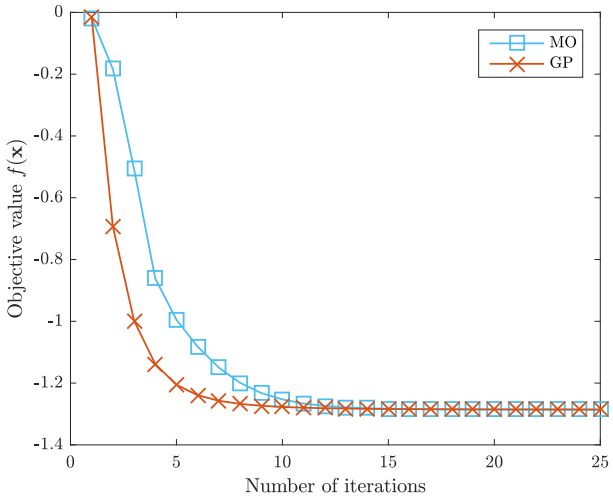

Fig. 3. Objective value versus normalized running time for an IRS-assisted downlink system when $M = 4$, $N = 100$, and $P = 5$ dBm.

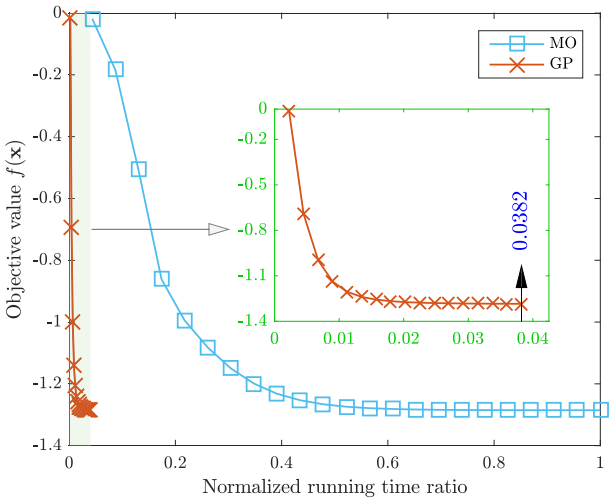

Fig. 4. Objective value versus number of iterations for an IRS-assisted downlink system when $M = 4$, $N = 100$, and $P = 5$ dBm.

time in Fig. 4 is *normalized* with respect to that of the MO-based algorithm for ease of comparison. Fig. 3 shows that the MO-based and GP-based algorithms converge to nearly the same objective value. This result confirms that the spectral efficiency achieved by the proposed GP-based algorithm is nearly the same as that obtained by the MO-based algorithm (Fig. 2). However, the average numbers of iterations required to achieve convergence for the MO-based and GP-based algorithms are 23.11 and 17.10, respectively. On the basis of the complexity analysis in Remark 3, the GP-based algorithm needs approximately only 21.14% of the computational complexity of the MO-based algorithm. Fig. 4 shows that the GP-based algorithm is significantly faster than the MO-based algorithm. From a detailed inspection, the proposed GP-based algorithm runs approximately 26.18 times faster than the MO-based algorithm. Figs. 2–4 exhibit that the proposed GP-based algorithm not only possesses low complexity but also nearly obtains the same spectral efficiency as

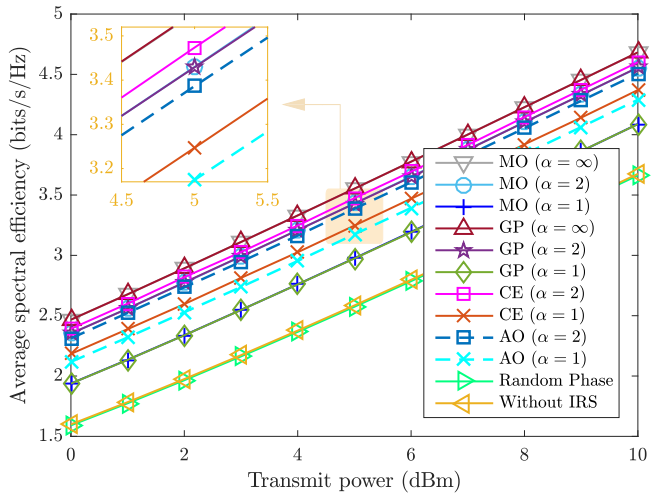

Fig. 5. Spectral efficiency versus transmit power for an IRS-assisted downlink system when $M = 4$ and $N = 100$.

the state-of-the-art MO-based algorithm. The required running time of the proposed GP-based algorithm can be significantly reduced.

C. Discrete Reflecting Coefficients

In this subsection, we investigate the spectral and energy efficiencies of the test algorithms by using low-resolution phase shifters. Fig. 5 presents the spectral efficiency versus the transmit power obtained by the MO-based, GP-based, MO-based [18], [19] and CE-based algorithms for $N = 100$ when low-resolution phase shifters are applied to the IRS. Here, we directly quantize each continuous phase shifter obtained by using the MO-based and GP-based algorithms to its nearest discrete value in $\mathcal{F}_\alpha$. As expected, the higher the phase shifter resolution is, the better the spectral efficiency is. Although the MO-based and GP-based algorithms with 2-bit phase shifters can achieve good performance, they suffer from significant performance loss when 1-bit phase shifters are employed. Moreover, the AO-based algorithm and the proposed CE-based algorithm can considerably mitigate the performance loss caused by coarse 1-bit phase shifters, for which the proposed CE-based algorithm still outperforms the AO-based algorithm. However, for 2-bit phase shifters, the spectral efficiency of the AO-based algorithm is inferior to those of the MO-based and GP-based algorithms. By contrast, the proposed CE-based algorithm performs better than the MO-based and GP-based algorithms for 2-bit phase shifters.

On the basis of the results obtained in Fig. 5, we further plot the energy efficiency of the test algorithms as a function of the transmission power in Fig. 6, where the energy efficiency is defined as [25]

$$\eta_{\text{eff}} = \frac{\mathsf{R}}{P_{\text{total}}} \quad \text{(bit/s/Hz/W)}. \tag{15}$$

Here, $P_{\text{total}} = P + P_{\text{BB}} + MP_{\text{RFchain}} + NP_{\alpha\text{-PS}}$ is the total power consumption; and P_{BB}, P_{RFchain}, and $P_{\alpha\text{-PS}}$ are the power consumptions of the baseband processor, RF chain, and α-bit

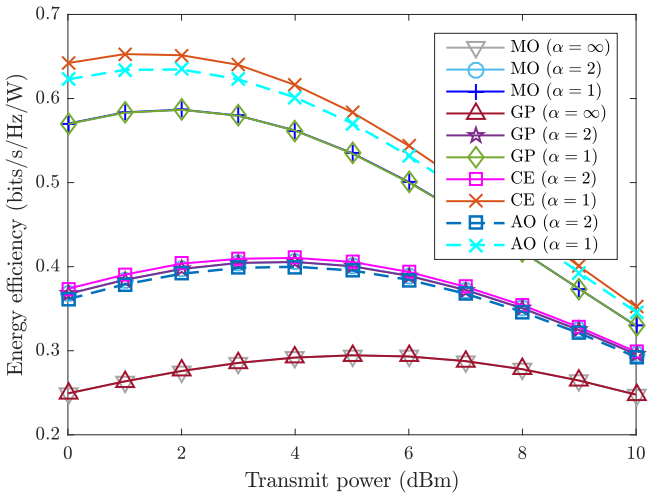

Fig. 6. Energy efficiency versus transmit power for an IRS-assisted downlink system when $M = 4$ and $N = 100$.

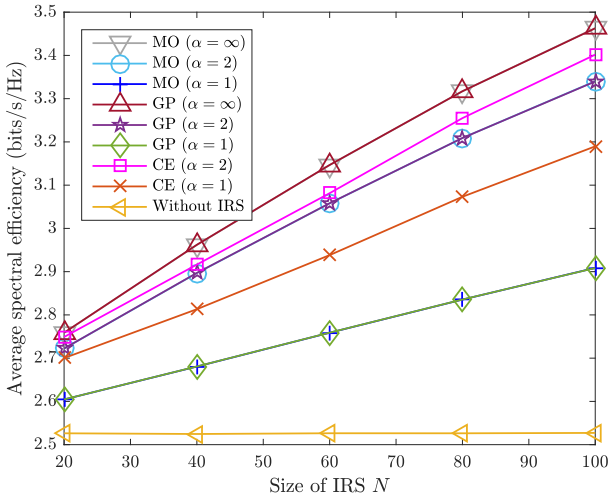

Fig. 8. Spectral efficiency versus number of phase shifters N for an IRS-assisted downlink system when $M = 4$ and $P = 5$ dBm.

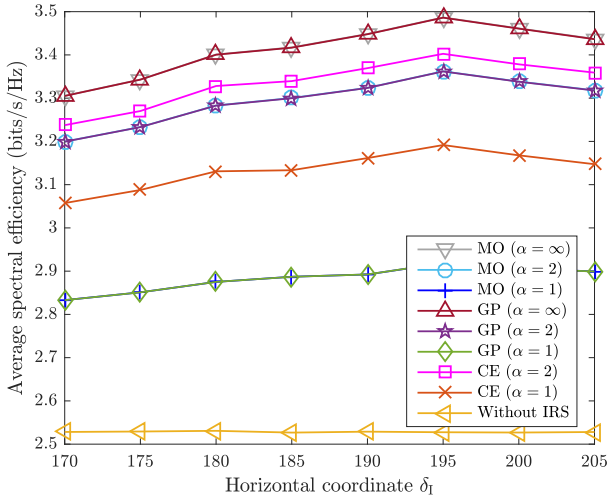

Fig. 7. Spectral efficiency versus the horizontal coordinate of IRS δ_{I} for an IRS-assisted downlink system when $M = 4$, $N = 100$, and $P = 5$ dBm.

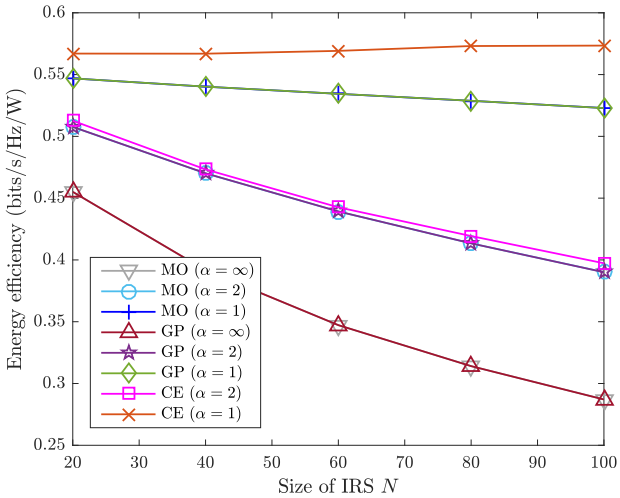

Fig. 9. Energy efficiency versus number of phase shifters N for an IRS-assisted downlink system when $M = 4$ and $P = 5$ dBm.

phase shifter, respectively. In the simulation, the power consumption values for these components are set as $P_{\mathrm{BB}} = 200$ mW, $P_{\mathrm{RFchain}} = 300$ mW, $P_{\text{1-PS}} = 10$ mW, $P_{\text{2-PS}} = 40$ mW, and $P_{\infty\text{-PS}} = 75$ mW [26]. We observe that the proposed CE-based algorithm can achieve higher energy efficiency than the others, especially when 1-bit phase shifters are employed.

D. Effect of IRS Deployment

In this subsection, we investigate the effects of IRS deployment locations and user position by moving the IRS from $(170\text{ m}, 0\text{ m})$ to $(205\text{ m}, 0\text{ m})$. Here, we denote the horizontal coordinate of IRS by δ_{I} for ease of presentation. Fig. 7 presents the spectral efficiency versus the horizontal coordinate of the IRS obtained by different algorithms. As expected, increasing δ_{I} from 200 m to 205 m decreases the spectral efficiency due to the increase in the path-losses of the AP-IRS and IRS-user channels. By contrast, decreasing from 200 m to 170 m decreases the path-loss of the AP-IRS channel and increases that of the IRS-user channel. Considering that the path-loss of the IRS-assisted channel is the product of the path losses of the AP-IRS and IRS-user channels, we observe that the spectral efficiency first increases and then decreases when δ_{I} drops from 200 m to 170 m. For a fixed resolution of α bits, the proposed CE-based algorithm still performs better than the conventional MO-based algorithm regardless of the IRS deployment.

E. Effect of Size of IRS

In this subsection, we investigate the effect of the size of the IRS. Figs. 8 and 9 respectively display the spectral and energy efficiencies as a function of the number of phase shifters N. Here, we set the total transmitted power $P = 5$ dBm. As shown in Fig. 8, the spectral efficiency improves with increasing N for the MO-based, the GP-based, and the CE-based algorithms. In addition, the proposed GP-based algorithm achieves nearly the

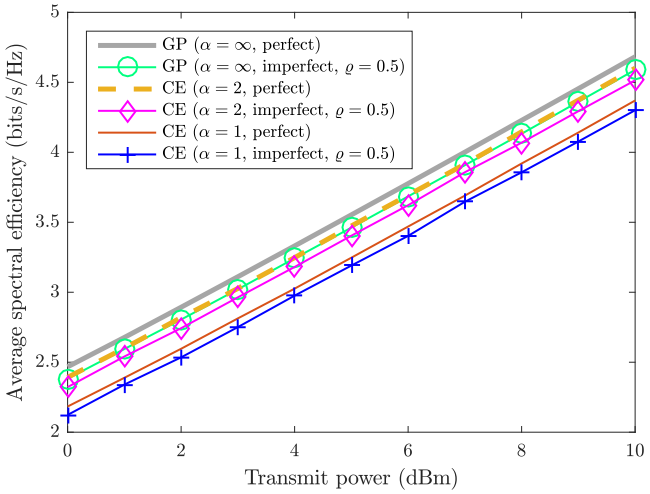

Fig. 10. Spectral efficiency versus transmit power for an IRS-assisted downlink system when $M = 4$ and $N = 100$ under *imperfect* channel state information setup.

same performance as the MO-based algorithm under the same resolution of phase shifters. Moreover, the proposed CE-based algorithm can improve the spectral efficiency performance of the MO-based and the GP-based algorithms when low-resolution phase shifters are applied to the IRS. These results show the same performance trends as those exhibited in Fig. 5. Although increasing N consumes much power, the energy efficiency of the proposed CE-based algorithm is better than that of the others, as shown in Fig. 9. Furthermore, we observe that the proposed CE-based algorithm is *not* highly sensitive to the size of the IRS.

F. Effect of Channel Estimation Error

Scholars have assumed that CSI can be perfectly known without any estimation errors [14]–[17]. Although several efficient channel estimation algorithms with high accuracy have been proposed for IRS-assisted wireless communication systems (e.g., [27], [28]), the channel estimation error should also be included to verify the robustness of the algorithms. Therefore, we investigate the behavior of the proposed algorithms by considering the channel estimation error. Based on the channel model in (1), (13), and (14), only the small-scale fading variables $\mathbf{h}_{\mathrm{d}}$, $\bar{\mathbf{G}}$, and $\bar{\mathbf{h}}_{\mathrm{r}}$ must be estimated in every frame. Following the channel estimation error model adopted in [24], [29]–[31], we assume that the estimated error of the aforementioned small-scale fading variables follows a zero-mean complex Gaussian distribution. In addition, we also assume that each element of these variables has the same normalized mean-square error given by [24]

$$\varrho = \frac{\mathrm{E}\{|\varpi - \widehat{\varpi}|^2\}}{\mathrm{E}\{|\widehat{\varpi}|^2\}}, \tag{16}$$

where ϖ represents one element in the above variables and $\widehat{\varpi}$ is the estimated version of ϖ. The graph in Fig. 10 presents the spectral efficiency versus the transmit power obtained by the GP-based and CE-based algorithms for $N = 100$ under *imperfect* CSI; the spectral efficiency curve of the GP-based algorithm with perfect CSI is replotted from Fig. 2 and the spectral efficiency curve of the CE-based algorithm with perfect CSI is replotted from Fig. 5 for ease of comparison. Given that the maximum value of ϱ in [24] is set to be $\varrho = 0.5$, we focus on the scenario where $\varrho = 0.5$. Fig. 10 demonstrates that the proposed GP-based and CE-based algorithms can still be applied for an imperfect CSI because their performance degradation levels are small.

VI. Conclusion

This study proposed two algorithms, namely, the GP-based and CE-based algorithms, to optimize the reflect beamforming in an IRS-assisted single-user MISO downlink system. The GP-based algorithm is aimed at reducing the computational and time complexities of the state-of-the-art MO-based algorithm while the CE-based algorithm is aimed at alleviating the performance loss caused by the use of low-resolution (e.g., 1–2 bits) phase shifters. Our simulation results demonstrate that the proposed GP-based algorithm provides indistinguishable spectral efficiency performance relative to the state-of-the-art MO-based algorithm at a low complexity while being about 26.18 times faster than the MO-based algorithm. Moreover, the proposed CE-based algorithm performs better than the test algorithms in terms of spectral and energy efficiency for various system configurations. In the future, we plan to extend the proposed GP-based and CE-based algorithms to multiuser scenarios.

Appendix A
Proof of Proposition 1

As described in Section III, the gradient of the objective function in (5a) can be expressed as $\nabla f(\mathbf{x}) = -2(\mathbf{A}\mathbf{x} + \mathbf{b})$. Then, we have

$$\|\nabla f(\mathbf{x}) - \nabla f(\mathbf{v})\|_2^2 = \|2\mathbf{A}(\mathbf{x} - \mathbf{v})\|_2^2 \overset{(a)}{\leq} 4\|\mathbf{A}\|_2^2\|\mathbf{x} - \mathbf{v}\|_2^2 \overset{(b)}{=} 4\lambda_{\max}\|\mathbf{x} - \mathbf{v}\|_2^2 \overset{(c)}{\leq} \frac{1}{\mu}\|\mathbf{x} - \mathbf{v}\|_2^2, \tag{17}$$

where (a) follows the fact of $\|\mathbf{A}(\mathbf{x} - \mathbf{v})\|_2^2 \leq \|\mathbf{A}\|_2^2\|\mathbf{x} - \mathbf{v}\|_2^2$, (b) uses the definition of matrix spectral norm, i.e., $\|\mathbf{A}\|_2^2 = \lambda_{\max}$, and (c) is obtained by choosing the stepsize satisfying $\mu \leq \frac{1}{4\lambda_{\max}}$. (17) demonstrates that $\nabla f(\mathbf{x})$ is Lipschitz continuous gradient with parameter $\frac{1}{\mu}$ and thus has the following property:

$$f(\mathbf{x}) \leq \underbrace{f(\mathbf{d}) + \nabla f(\mathbf{v})^{\top}(\mathbf{x} - \mathbf{v}) + \frac{1}{2\mu}\|\mathbf{x} - \mathbf{v}\|_2^2}_{\triangleq g(\mathbf{x},\mathbf{v})}, \tag{18}$$

where $g(\mathbf{x}, \mathbf{v})$ is the quadratic upper bound surrogate function of $f(\mathbf{x})$. Then, a two-step iterative majorization-minimization (MM) algorithmic framework [32] is applied to solve problem (5). For each iteration t, the first step of the MM framework is to find $\mathbf{d}$ such that the difference between the surrogate function and the objective function is minimized at the current point $\mathbf{x}^{(t)}$. Considering the equality of (18) holds if and only if $\mathbf{v} = \mathbf{x}$, we update $\mathbf{v}$ as $\mathbf{v}^{(t)} = \mathbf{x}^{(t)}$ and we have $f(\mathbf{x}^{(t)}) = g(\mathbf{x}^{(t)}, \mathbf{v}^{(t)})$. Then, in the second step of the MM framework, we optimize the

surrogate function with respect to $\mathbf{x}$ by fixing $\mathbf{v}^{(t)} = \mathbf{x}^{(t)}$, i.e.,

$$\begin{aligned}\mathbf{x}^{(t+1)} &= \underset{\mathbf{x}\in\mathcal{S}}{\operatorname{argmin}}\ g(\mathbf{x}, \mathbf{x}^{(t)}) \\ &= \underset{\mathbf{x}\in\mathcal{S}}{\operatorname{argmin}}\ \mathbf{x}^\top \nabla f(\mathbf{x}^{(t)}) + \frac{1}{2\mu}\|\mathbf{x}\|_2^2 - \frac{1}{\mu}\mathbf{x}^\top \mathbf{x}^{(t)} \\ &= \underset{\mathbf{x}\in\mathcal{S}}{\operatorname{argmin}}\ \frac{1}{2\mu}\left[\|\mathbf{x}\|_2^2 - 2\mathbf{x}^\top\left(\mathbf{x}^{(t)} - \mu\nabla f(\mathbf{x}^{(t)})\right)\right] \\ &= \underset{\mathbf{x}\in\mathcal{S}}{\operatorname{argmin}}\ \frac{1}{2\mu}\left\|\mathbf{x} - \left(\mathbf{x}^{(t)} - \alpha\nabla f(\mathbf{x}^{(t)})\right)\right\|_2^2 \\ &= \underset{\mathbf{x}\in\mathcal{S}}{\operatorname{argmin}}\ \frac{1}{2\mu}\left\|\mathbf{x} - \boldsymbol{\zeta}^{(t+1)}\right\|_2^2 = e^{\mathrm{j}\measuredangle\boldsymbol{\zeta}^{(t+1)}}, \end{aligned} \tag{19}$$

which is in the manner of the updating process in (8). Therefore, we can conclude that the sequence $\{f(\mathbf{x}^{(t)})\}$ generated by the GP algorithm is non-increasing since

$$f(\mathbf{x}^{(t)}) = g(\mathbf{x}^{(t)}, \mathbf{v}^{(t)}) \overset{(a)}{\geq} g(\mathbf{x}^{(t+1)}, \mathbf{v}^{(t)}) \overset{(b)}{\geq} f(\mathbf{x}^{(t+1)}), \tag{20}$$

where (a) follows from (19), and (b) follows from (18). ■

APPENDIX B
PROOF OF PROPOSITION 2

Given L^{elite} elite solutions $\{\mathbf{x}_{[\ell]}^{(t)}\}_{\ell=1}^{L^{\text{elite}}}$, the optimal updating rule of parameter matrix $\mathbf{P}$ in the sense of the smallest Kullback–Leibler divergence is equivalent to solving the following stochastic program [20]

$$\max_{\mathbf{P}}\ \frac{1}{L}\sum_{\ell=1}^{L^{\text{elite}}} \ln \mathscr{P}(\mathbf{x}_{[\ell]}^{(t)}; \mathbf{P}). \tag{21}$$

However, since the sum total probability of an element in set $\mathcal{F}_\alpha$ being assigned to each phase shifter is 1, the rows of $\mathbf{P}$ sum up to 1, i.e., $\sum_{k=1}^{|\mathcal{F}_\alpha|} p_{nk} = 1$ for $n = 1, \ldots, N$. This constraint can be enforced in maximizing (21) by using the Lagrangian function

$$\mathscr{L} = \frac{1}{L}\sum_{\ell=1}^{L^{\text{elite}}} \ln \mathscr{P}(\mathbf{x}_{[\ell]}^{(t)}; \mathbf{P}) + \sum_{n=1}^{N}\gamma_n\left(\sum_{k=1}^{|\mathcal{F}_\alpha|} p_{nk} - 1\right), \tag{22}$$

where $\{\gamma_n\}_{n=1}^N$ are the Lagrangian multipliers.

Differentiating (22) and setting $\frac{\partial \mathscr{L}}{\partial p_{nk}} = 0$, we have

$$\frac{1}{L}\sum_{\ell=1}^{L^{\text{elite}}} \frac{\partial}{\partial p_{nk}} \ln \mathscr{P}(\mathbf{x}_{[\ell]}^{(t)}; \mathbf{P}) + \gamma_n = 0. \tag{23}$$

From (9), the partial derivative of $\ln \mathscr{P}(\mathbf{x}_{[\ell]}^{(t)}; \mathbf{P})$ is given by

$$\begin{aligned}\frac{\partial}{\partial p_{nk}} \ln \mathscr{P}(\mathbf{x}_{[\ell]}^{(t)}; \mathbf{P}) &= \prod_{n=1}^{N}\sum_{k=1}^{|\mathcal{F}_\alpha|} \mathbb{1}_{\{\mathcal{I}_n(\mathbf{x}_{[\ell]}^{(t)}) = e^{\mathrm{j}k\Delta}\}} \frac{\partial}{\partial p_{nk}} \ln p_{nk} \\ &= \frac{\mathbb{1}_{\{\mathcal{I}_n(\mathbf{x}_{[\ell]}^{(t)}) = e^{\mathrm{j}k\Delta}\}}}{p_{nk}}. \end{aligned} \tag{24}$$

Substituting (24) into (23), we get

$$\frac{1}{L}\sum_{\ell=1}^{L^{\text{elite}}} \frac{\mathbb{1}_{\{\mathcal{I}_n(\mathbf{x}_{[\ell]}^{(t)}) = e^{\mathrm{j}k\Delta}\}}}{p_{nk}} + \gamma_n = 0$$

$$\Leftrightarrow\ \frac{1}{L}\sum_{\ell=1}^{L^{\text{elite}}} \mathbb{1}_{\{\mathcal{I}_n(\mathbf{x}_{[\ell]}^{(t)}) = e^{\mathrm{j}k\Delta}\}} + \gamma_n p_{nk} = 0. \tag{25}$$

Summing (25) over $k = 1, \ldots, |\mathcal{F}_\alpha|$ together yields

$$\gamma_n = -\frac{L^{\text{elite}}}{L}. \tag{26}$$

Finally, by substituting (26) into (25), we get

$$p_{nk} = \frac{1}{L^{\text{elite}}}\sum_{\ell=1}^{L^{\text{elite}}} \mathbb{1}_{\{\mathcal{I}_n(\mathbf{x}_{[\ell]}^{(t)}) = e^{\mathrm{j}k\Delta}\}}, \tag{27}$$

which immediately implies (10). ■

ACKNOWLEDGMENT

The author would like to thank the Editor, Dr. Hai Lin, and all the anonymous Reviewers for their valuable comments and suggestions for enhancing the readability and technical quality of this article.

REFERENCES

[1] Q. Wu, S. Zhang, B. Zheng, C. You, and R. Zhang, "Intelligent Reflecting Surface Aided Wireless Communications: A tutorial," 2020, *arXiv:2007.02759*.
[2] C. Huang, A. Zappone, G. C. Alexandropoulos, M. Debbah, and C. Yuen, "Reconfigurable intelligent surfaces for energy efficiency in wireless communication," *IEEE Trans. Wirel. Commun.*, vol. 18, no. 8, pp. 4157–4170, Aug. 2019.
[3] Y.-C. Liang, R. Long, Q. Zhang, J. Chen, H. V. Cheng, and H. Guo, "Large intelligent surface/antennas (LISA): Making reflective radios smart," *J. Commun. Inf. Netw.*, vol. 4, no. 2, pp. 40–50, Jun. 2019.
[4] Q. Wu and R. Zhang, "Towards smart and reconfigurable environment: Intelligent reflecting surface aided wireless networ," *IEEE Commun. Mag.*, vol. 58, no. 1, pp. 106–112, Jan. 2020.
[5] H. Shen, W. Xu, S. Gong, Z. He, and C. Zhao, "Secrecy rate maximization for intelligent reflecting surface assisted multi-antenna communications," *IEEE Commun. Lett.*, vol. 23, no. 9, pp. 1488–1492, Sep. 2019.
[6] M. Cui, G. Zhang, and R. Zhang, "Secure wireless communication via intelligent reflecting surface," *IEEE Wirel. Commun. Lett.*, vol. 8, no. 5, pp. 1410–1414, Oct. 2019.
[7] X. Yu, D. Xu, and R. Schober, "Enabling secure wireless communications via intelligent reflecting surfaces," in *Proc. IEEE Glob. Commun. Conf.*, Waikoloa, HI, USA, Dec. 2019, pp. 1–6.
[8] X. Yu, D. Xu, Y. Sun, D. W. K. Ng, and R. Schober, "Robust and secure wireless communications via intelligent reflecting surfaces," *IEEE J. Sel. Area. Comm.*, vol. 38, no. 11, pp. 2637–2652, Nov. 2020.
[9] Q. Wu and R. Zhang, "Weighted sum power maximization for intelligent reflecting surface aided SWIPT," *IEEE Wirel. Commun. Lett.*, vol. 9, no. 5, pp. 586–590, May 2020.
[10] Q. Wu and R. Zhang, "Joint active and passive beamforming optimization for intelligent reflecting surface assisted SWIPT under QoS constraints," *IEEE J. Sel. Area. Comm.*, vol. 38, no. 8, pp. 1735–1748, Aug. 2020.
[11] C. Pan *et al.*, "Intelligent reflecting surface aided MIMO broadcasting for simultaneous wireless information and power transfer," *IEEE J. Sel. Area. Comm.*, vol. 38, no. 8, pp. 1719–1734, Aug. 2020.
[12] D. Mishra and H. Johansson, "Channel estimation and low-complexity beamforming design for passive intelligent surface assisted MISO wireless energy transfer," in *Proc. IEEE Int. Conf. Acoust., Speech, Signal Process.*, Brighton, U.K., May 2019, pp. 4659–4663.
[13] G. Zhou, C. Pan, H. Ren, K. Wang, and A. Nallanathan, "Intelligent reflecting surface aided multigroup multicast MISO communication systems," *IEEE Trans. Signal Process.*, vol. 68, pp. 3236–3251, 2020.
[14] Q. Wu and R. Zhang, "Intelligent reflecting surface enhanced wireless network: Joint active and passive beamforming design," in *Proc. IEEE Glob. Commun. Conf.*, Abu Dhabi, United Arab Emirates, Dec. 2018, pp. 1–6.

[15] Q. Wu and R. Zhang, "Intelligent reflecting surface enhanced wireless network via joint active and passive beamforming," *IEEE Trans. Wirel. Commun.*, vol. 18, no. 11, pp. 5394–5409, Nov. 2019.
[16] X. Yu, D. Xu, and R. Schober, "MISO wireless communication systems via intelligent reflecting surfaces," in *Proc. IEEE Int. Conf. Commun.*, Changchun, China, Aug. 2019, pp. 735–740.
[17] X. Yu, D. Xu, and R. Schober, "Optimal beamforming for MISO communications via intelligent reflecting surfaces," in *Proc. IEEE Int. Workshop Signal Process. Adv. Wireless Commun.*, Atlanta, GA, USA, May 2020, pp. 1–6.
[18] Q. Wu and R. Zhang, "Beamforming optimization for intelligent reflecting surface with discrete phase shifts," in *Proc. IEEE Int. Conf. Acoust., Speech Signal Process.*, Brighton, U.K., May 2019, pp. 7830–7833.
[19] Q. Wu and R. Zhang, "Beamforming optimization for wireless network aided by intelligent reflecting surface with discrete phase shifts," *IEEE Trans. Commun.*, vol. 68, no. 3, pp. 1838–1851, Mar. 2020.
[20] R. Y. Rubinstein and D. P. Kroese, *The Cross-Entropy Method: A Unified Approach to Combinatorial Optimization, Monte-Carlo Simulation and Machine Learning.* Berlin, Germany: Springer-Verlag, 2004.
[21] D. P. Bertsekas, "*Nonlinear Programming*," Belmont, MA, USA: Athena Scientific, 1999.
[22] J.-C. Chen, "Manifold optimization approach for data detection in massive multiuser MIMO systems," *IEEE Trans. Veh. Technol.*, vol. 67, no. 4, pp. 3652–3657, Apr. 2018.
[23] A. Costa, O. D. Jones, and D. Kroese, "Convergence properties of the cross-entropy method for discrete optimization," *Oper. Res. Lett.*, vol. 35, no. 5, pp. 573–580, Sep. 2007.
[24] H. Guo, Y.-C. Liang, J. Chen, and E. G. Larsson, "Weighted sum-rate maximization for reconfigurable intelligent surface aided wireless networks," *IEEE Trans. Wirel. Commun.*, vol. 19, no. 5, pp. 3064–3076, May 2020.
[25] R. Mèndez-Rial, C. Rusu, N. Gonzàlez-Prelcic, A. Alkhateeb, and R. W. Heath, Jr., "Hybrid MIMO architectures for millimeter wave communications: Phase shifters or switches?," *IEEE Access*, vol. 4, pp. 247–267, 2016.
[26] Z. Wang, Q. Liu, M. Li, and W. Kellerer, "Energy efficient analog beamformer design for mmWave multicast transmission," *IEEE Trans. Green Commun. Netw.*, vol. 3, no. 2, pp. 552–564, Jun. 2019.
[27] B. Zheng and R. Zhang, "Intelligent reflecting surface-enhanced OFDM: Channel estimation and reflection optimization," *IEEE Wirel. Commun. Lett.*, vol. 9, no. 4, pp. 518–522, Apr. 2020.
[28] J.-M. Kang, "Intelligent reflecting surface: Joint optimal training sequence and refection pattern," *IEEE Commun. Lett.*, vol. 24, no. 8, pp. 1784–1788, Aug. 2020.
[29] C. Wang and R. D. Murch, "Adaptive downlink multi-user MIMO wireless systems for correlated channels with imperfect CSI," *IEEE Trans. Wirel. Commun.*, vol. 5, no. 9, pp. 2435–2446, Sep. 2006.
[30] T. Yoo and A. Goldsmith, "Capacity and power allocation for fading MIMO channels with channel estimation error," *IEEE Trans. Inf. Theory*, vol. 52, no. 5, pp. 2203–2214, May 2006.
[31] A. Dabbagh and D. Love, "Multiple antenna MMSE based downlink precoding with quantized feedback or channel mismatch," *IEEE Trans. Commun.*, vol. 56, no. 11, pp. 1859–1868, Nov. 2008.
[32] Y. Sun, P. Babu, and D. P. Palomar, "Majorization-minimization algorithms in signal processing, communications, and machine learning," *IEEE Trans. Signal Process.*, vol. 65, no. 3, pp. 794–816, Feb. 2017.

Jung-Chieh Chen (Member, IEEE) received the Ph.D. degree in communications engineering from National Tsing Hua University, Hsinchu, Taiwan, in 2005.

Since August 2005, he has been with the Department of Electrical Engineering (formerly known as Department of Optoelectronics and Communication Engineering), National Kaohsiung Normal University, Kaohsiung, Taiwan, as an Assistant Professor, where he was promoted as an Associate Professor, a Full Professor, and a Distinguished Professor, in March 2009, March 2012, and August 2020, respectively. His research interests include wireless communication systems, radio resource management, the stochastic optimization methods, and signal processing for communications. He was the recipient of the IET Outstanding Editor Award, in 2019. He was also the recipient of the Best Service Award from the IEEE Tainan Section, in 2020.

Prof. Chen currently is an Editor for the IEEE TRANSACTIONS ON VEHICULAR TECHNOLOGY and the IEEE WIRELESS COMMUNICATIONS LETTERS. He is also an Associate Editor for *IET Signal Processing*.